Journal of Materials Chemistry B

PAPER

View Article Online
View Journal | View Issue

Cite this: J. Mater. Chem. B, 2014, 2, 3263

An electrochemiluminescence biosensor for sensitive and selective detection of Hg^{2+} based on π–π interaction between nucleotides and ferrocene–graphene nanosheets†

Bangrong Zhuo,‡[a] Yuqin Li,‡[b] An Zhang,[a] Fushen Lu,[a] Yaowen Chen[c] and Wenhua Gao*[ac]

Received 20th January 2014
Accepted 29th March 2014

DOI: 10.1039/c4tb00115j

www.rsc.org/MaterialsB

A solid-state electrochemiluminescence (ECL) biosensor based on a DNA-modified electrode platform that depends on the variation of π–π interaction before and after the binding of target analytes is put forward. The single-stranded DNA (ssDNA) probe was successfully assembled on the surface of a glassy carbon electrode (GCE), which was pre-modified with $Ru(bpy)_3^{2+}$ complex and gold nanoparticles (GNPs). The ssDNA probe could strongly adsorb graphene due to the strong π–π interaction between nucleotides and graphene (GN), while in the presence of Hg^{2+}, the conformational transformation of DNA from a single-stranded to a double-stranded structure resulted in inhibited adsorption of GN. With thymine (T)-rich ssDNA as a Hg^{2+} probe, we prepared the ECL biosensor by using ferrocene–graphene (Fc–GN) as a quenching unit to quench the ECL emission of $Ru(bpy)_3^{2+}$, and the Hg^{2+} can be detected by quenching efficiency transformation when the Fc–GN gets away from $Ru(bpy)_3^{2+}$. The biosensor exhibited a sensitive response to various ranges of concentration of Hg^{2+} with a detection limit of 18 pM. The ECL biosensor held great promise in the highly sensitive and selective detection of Hg^{2+} in natural water.

1. Introduction

Mercuric ion (Hg^{2+}) is a major environmental pollutant, and it is estimated by the United Nations Environment Programme (UNEP) that *ca.* 7500 tons of mercury are released into the environment annually. Mercuric ion is known for its high toxicity and can cause many toxic effects to the human body. It affects the immune system, alters genetic and enzyme systems, damages the nervous system, and can result in several diseases including acrodynia, kidney failure as well as Minamata disease.[1–3] To date, several kinds of technologies have been developed for detecting Hg^{2+} ions, such as atomic absorption spectroscopy, cold vapor atomic fluorescence spectrometry and gas chromatography.[4] Although these techniques are quite highly sensitive, selective and accurate for Hg^{2+} assay, many of these methods require complicated and multistep sample preparations or sophisticated instrumentations. Above all, these methods couldn't meet the requirement of quick detection of Hg^{2+}. It is reported that Hg^{2+} could specifically bind two DNA thymine (T) bases and promote the T–T mismatch forming stable base pairs.[5,6] According to this principle, biosensors based on electrochemiluminescence (ECL) for detection of Hg^{2+} have been developed due to their simple instrumentation and rapid response to the target substances.

Electrochemiluminescence is a well-known detection method that provides high sensitivity and selectivity through the generation of an optical signal triggered by an electrochemical reaction.[7] As the most widely presented ECL reagent, tris(2,2′-bipyridine)ruthenium(II) [$Ru(bpy)_3^{2+}$] has attracted much attention during the past several decades due to its unique advantages of good electrochemical stability, high ECL efficiency and the convenience in coupling it with various measurement techniques.[8,9] However, the continuous consumption of $Ru(bpy)_3^{2+}$ in solution limits the widespread application of $Ru(bpy)_3^{2+}$ ECL sensors.[10] Since $Ru(bpy)_3^{2+}$ can be regenerated during the ECL reaction, it is possible and necessary to find a convenient method to realize $Ru(bpy)_3^{2+}$ immobilization on the electrode surface to reduce the consumption of expensive ECL reagent and simplify experimental design.[11,12] Up to now, many methods have been reported immobilization of $Ru(bpy)_3^{2+}$ on the electrode surface. For example, $Ru(bpy)_3^{2+}$ has been incorporated with Langmuir–Blodgett films,[13] polymer films[14] and sol–gel composites.[15] Besides, our previous work has

[a]Department of Chemistry, Shantou University, Shantou, Guangdong 515063, P. R. China. E-mail: whgao@stu.edu.cn; Fax: +86-22-82903941; Tel: +86-22-86502774
[b]Department of Pharmacy, Taishan Medicine College, Taian, Shandong 271016, P. R. China
[c]Analysis & Testing Center, Shantou University, Shantou, Guangdong 515063, P. R. China

† Electronic supplementary information (ESI) available. See DOI: 10.1039/c4tb00115j

‡ Bangrong Zhuo and Yuqin Li contributed equally to this work.

developed a novel approach to immobilize the $Ru(bpy)_3^{2+}$ by a graphene film *via in situ* wet-chemical reduction of graphene oxide (GO).[16] Nevertheless, these methods with the requirement of additional substances are complicated in terms of the experimental design. In another work, Soo Beng Khoo *et al.*[17] reported that $Ru(bpy)_3^{2+}$ complex molecules were directly attached to the solid glassy carbon surface of a glassy carbon electrode (GCE) without using any additional host matrices. Herein, we immobilized the $Ru(bpy)_3^{2+}$ on a GCE by a brief potentiostatic approach, which applied a high anodic potential on the bare GCE in the $Ru(bpy)_3^{2+}/KNO_3$ solution. The crackled glassy carbon oxide film was formed on surface of the GCE, and the co-deposition of the glassy carbon with the $Ru(bpy)_3^{2+}$ complex led to stable immobilization of the $Ru(bpy)_3^{2+}$ complex.

Graphene (GN), as a one-atom-thick sheet of sp^2-bonded carbon atoms in a closely packed honeycomb lattice with unique electrical conductivity, extraordinary surface area,[18] high potential for mass production and easy functionalization,[19] has revealed enormously promising gateways for rapid progress in various scientific and technological fields, such as biophysics and biotechnology.[20–23] Particularly, by virtue of the high surface area, high π-conjunction and hydrophobic properties, GN can provide a platform for immobilizing organic and inorganic molecules, which promotes the development of graphene-based sensors.[24,25] GN could be strongly adsorbed on the ssDNA probe due to the strong π–π stacking between nucleotides and GN, and the adsorption of GN was inhibited when the probe bound the specific target to form a double helix. The study on the unique interactions of GN and nucleotides has been well developed in electrochemical biosensing. Shaojun Dong *et al.*[26] designed an excellent electrochemical aptasensor by taking advantage of the ultrahigh electron transfer ability of GN and its unique GN/ssDNA interaction. However, the mechanism of the distinctive GN/ssDNA interaction has not been well employed to fabricate ECL biosensors. Thus, we designed a brief ultra-sensitive ECL biosensor preparation method by utilizing the ssDNA to adsorb the ferrocene–graphene nanosheets (Fc–GNs), and we used the Fc–GNs as quenching units to quench the ECL emission of $Ru(bpy)_3^{2+}$.

In the present work, a thiolated-ssDNA probe was successfully anchored on gold nanoparticles (GNPs) through a thiol–Au bond to assemble a monolayer of ssDNA on the surface of GCE. A thiolated 28-*mer* T-rich ssDNA was designed to capture Hg^{2+} in the light of the theory that Hg^{2+} could specifically bind two DNA thymine (T) bases and promote the T–T mismatch to form a stable base pair. As shown in Scheme 1, first, the GCE modified by $Ru(bpy)_3^{2+}$ complex molecules and GNPs formed a platform for the self-assembly of T-rich ssDNA. Secondly, the biosensing electrode was immersed into a certain concentration of Fc–GN solution. Due to the strong π–π interaction, the Fc–GN was adsorbed on the ssDNA and effectively quenched the ECL intensity of $Ru(bpy)_3^{2+}$ complex. Finally, in presence of Hg^{2+}, the T-rich ssDNA binding Hg^{2+} to form T–Hg^{2+}–T stable base pairs and get the conformational transition of ssDNA to C-type dsDNA coincided with the transformation of luminescence signal from "off" to "on". By employing this strategy, an ECL biosensor was successfully applied to the ultrasensitive detection of Hg^{2+} in natural water.

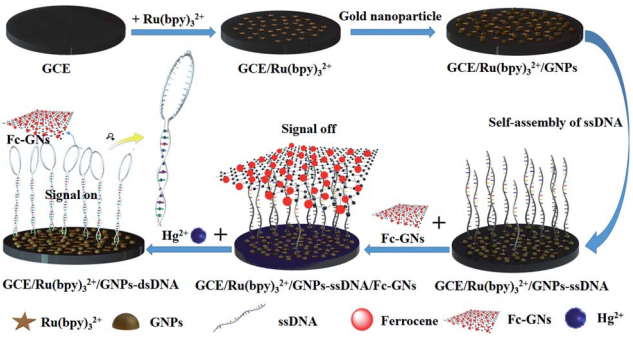

Scheme 1 Schematic illustration of the ECL biosensor for Hg^{2+} detection.

2. Experimental

2.1 Reagents and apparatus

Oligonucleotides were purchased from Sangon Bioengineering Ltd. Company (Shanghai, China), and the sequence is shown as follows:

5′-SH–$(CH_2)_6$–ATT CTT TGT TCT CCC CTG TTC TTT GTT T-3′

Tris (2,2′-bipyridyl) ruthenium(II) chloride hexahydrate, 2-mercaptohexanol (MCH), mercury nitrate ($Hg(NO_3)_2$) and other metal salts were purchased from Sigma-Aldrich (St. Louis, MO, USA). Tri-*n*-propylamine (TPrA), ferrocene–carboxaldehyde (FcCHO) and tetrachloroauric(III) acid tetrahydrate ($HAuCl_4 \cdot 4H_2O$) were obtained from Aladdin Chemical Reagent Co. Ltd. (Shanghai, China). Sodium borohydride ($NaBH_4$) was obtained from Beijing Chemical Factory (Beijing, China). Ethylenediamine (ED) and *N*,*N*′-dicyclohexyl-carbodiimide (DCC, 99%) were purchased from Sinopharm Chemical Reagent Co. Ltd. (Shanghai, China). All other chemicals not mentioned here were of analytical reagent grade and were used as received. Millipore Milli-Q water (18 ΩM cm) supplied by a Millipore Milli-Q water purification system (Bedford, MA, USA) was used throughout the process. The working solutions were prepared by diluting the stock solution with phosphate buffer solution (PBS, pH 7.50, 0.10 M NaCl + 0.10 M NaH_2PO_4/Na_2HPO_4) and deionized water. All measurements were carried out at room temperature, 24 ± 2 °C.

A traditional three-electrode system composed of a bare GCE (3 mm in diameter) or biosensor as the working electrode, a platinum wire as the counter electrode and a Ag/AgCl (1 M KCl) as the reference electrode was applied in a 10 mL glassy analytical cell. Cyclic voltammetry (CV) curves and electrochemical impedance spectroscopy (EIS) were measured with an IM6ex electrochemical workstation (Zahner IM6ex, Germany). ECL detections were carried out with a MPI-B ECL Analyzer Systems (Remax, China). Fourier Transform-Infrared (FT-IR) spectra were recorded on a Magna 750 FTIR spectrophotometer (Nicolet, USA) as KBr pellets. A scanning electron microscope (SEM, JSM-6360LA, JEOL, Japan) was used to observe the modified electrodes. Atomic force microscopy (AFM) was

performed on a Digital Instruments Nanoscope IIIa (Veeco, CA, USA). The electron micrographs of GO and Fc–GNs were taken by using a transmission electron microscope (TEM, JEM-1400, JEOL, Japan). A PHS-3CA precision pH meter (Dapu, China) was used in the experiment. Sample analysis was performed with an atomic fluorescence spectrometer (AFS-230E, China).

2.2 Electrode cleaning, conditioning and electrochemical deposition of $Ru(bpy)_3^{2+}$ and GNPs

GCEs with a glassy carbon (GC) rod diameter of 3 mm were polished with 0.3 μm and 0.05 μm alumina slurry (Al_2O_3) sequentially on a polishing cloth. The electrodes were fully rinsed after each polishing step and finally sonicated in deionized water and anhydrous ethanol for 5 min each, followed by electrochemical conditioning by potential scanning from −0.2 V to 1.6 V in 0.5 M H_2SO_4 for at least five complete scans at 100 mV s^{-1} until the reproducible cyclic voltammogram was obtained. Then the electrode was immediately used for deposition modification after a rinse step.

The immobilization of $Ru(bpy)_3^{2+}$ was based on a modified electrochemical method.[17] The $Ru(bpy)_3^{2+}$ complex molecules were electrodeposited on the glassy carbon surface of a GCE by applying a high anodic potential of 1.8 V for 300 s in 0.1 mM $Ru(bpy)_3^{2+}$ complex in 0.01 M potassium nitrate (KNO_3) solution. After a rinse step with deionized water, the GCE/$Ru(bpy)_3^{2+}$ electrode was immersed into 100 μM of $HAuCl_4$ solution in 5 mL of 0.5 M KNO_3 and applying a 5 s potential step from 1.1 to −1.0 V to deposit the GNPs according to our previous experimental work.[27]

2.3 Preparation of Fc–GNs

GO was prepared from graphite flakes based on a modified Hummers method.[28] Fc–GNs were synthesized according to the previously reported method.[29] The Fc–GNs were characterized by FT-IR spectroscopy (Fig. S1†), AFM and TEM images (Fig. S2†) so as to verify that ferrocene (Fc) was indeed grafted onto the surface of graphene nanosheets. More details of the Fc–GN synthesis can be found in the ESI.†

2.4 Fabrication of biosensing electrode

The electrode modified by electrodeposited $Ru(bpy)_3^{2+}$ complex molecules and GNPs was first immersed in the 10 μM DNA solution in order to assemble a monolayer of ssDNA probe through the thiol–Au bond between thiolated-DNA probes and GNPs. The distribution and orientation of ssDNA was well controlled by the GNPs rather than simply sprawling the ssDNA strands on the planar gold electrode, according to our previous experimental work.[27] The assembly process was kept for at least 3 h at room temperature, followed by thorough washing in a stirred solution of PBS for 20 min to remove any weakly bound DNA strands. In order to obtain well-aligned DNA monolayers with the probe strands nearly perpendicular to the surface of the electrode, the electrode was finally treated with 1 mM MCH solution for 1 h at room temperature and washed again in the stirred solution of PBS solution for 20 min. Then the electrode was immersed in the 2.0 mg mL^{-1} Fc–GN solution for at least 1 h. Finally, the modified electrode was carefully washed to remove the unfixed Fc–GN aggregates with deionized water, and then the ECL biosensor was obtained.

2.5 ECL measurement of Hg^{2+}

Various concentrations of Hg^{2+} were prepared for determining the sensitivity of this ECL biosensor by serial dilution of the $Hg(NO_3)_2$ stock solution. After a pre-scan to record the luminescence intensity of the "signal-off" sensor, the sensor was immersed into 100 μL PBS containing certain concentration of Hg^{2+} for 30 min at room temperature followed by washing for at least 5 min with 0.1 M PBS and deionized water to remove any unbound substances.

The ECL determinations were performed at room temperature and in CV mode with continuous potential scanning from 0.2 V to 1.25 V at a scanning rate of 100 mV s^{-1} applied to achieve ECL signals in 0.1 M PBS (pH 7.50, 0.10 M NaCl + 0.10 M NaH_2PO_4/Na_2HPO_4) containing 0.1 M TPrA. The supersaturated TPrA solution was prepared according to a previous protocol.[30] A negative high voltage of −800 V was supplied to the photomultiplier for luminescence intensity determination.

3. Results and discussion

3.1 Characterization of the electrode electrodeposited $Ru(bpy)_3^{2+}$ and GNPs

In order to obtain information on the change of the GCE and after electrodeposition of the $Ru(bpy)_3^{2+}$ complex molecules and GNPs, cyclic voltammetry (CV) curves were carried out. The bare GCE and the modified GCE were used for CV measurement. As shown in Fig. 1A, curve a exhibited the bare GCE in 0.05 M H_2SO_4 solution at the scan rate of 100 mV s^{-1} and the curve was smooth without an obvious reversible peak. Following the electrodeposition of the GNPs on the surface of the GCE, curve b exhibited a reduction potential at 0.68 V and indicated that the GNP modified GCE was obtained. As shown in Fig. 1B, after applying a high anodic potential of 1.8 V on the bare GCE for 300 s in $Ru(bpy)_3^{2+}/KNO_3$ solution, a reversible peak ($E^{0\prime} = 1.03$ V) was observed (curve a), indicating that the $Ru(bpy)_3^{2+}$ complex molecules were immobilized on the glassy carbon surface of the GCE. Curve b showed the $Ru(bpy)_3^{2+}$ and GNPs modified GCE (GCE/$Ru(bpy)_3^{2+}$/GNPs) in 0.05 M H_2SO_4 solution at the scan rate of 100 mV s^{-1}. Another oxidation current peak at 1.23 V and reduction potential at 0.52 V were also observed in curve d, and this was probably due to the fact that the electrodeposition of GNPs affected the feature of the GCE/$Ru(bpy)_3^{2+}$ electrode. Continuous cycles of the GCE/$Ru(bpy)_3^{2+}$/GNPs electrode showed excellent stability, confirming that the $Ru(bpy)_3^{2+}$ complex molecules were strongly bound on the glassy carbon surface of the GCE. Furthermore, this conclusion was also supported by the SEM images of the modified GCE. It could be found that the surface of the bare GCE (Fig. 2A) was smooth, while the GCE showed crackled microstructure after applying a high anodic potential of 1.8 V (Fig. 2B). It can be interpreted that $Ru(bpy)_3^{2+}$ could be electrodeposited with the pre-modified GCE and exert a stable

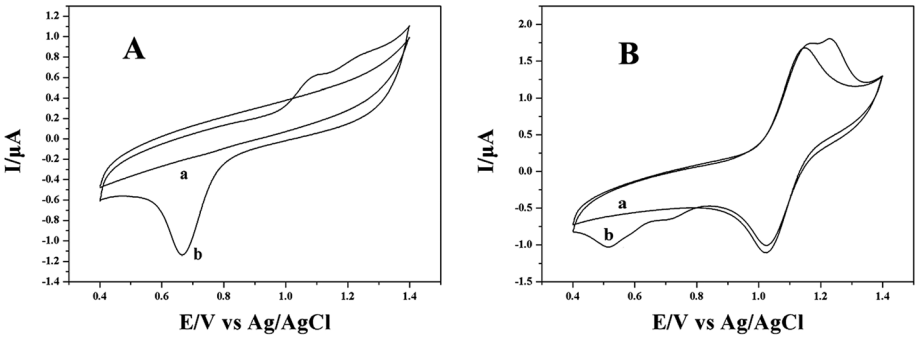

Fig. 1 Continuous cyclic voltammograms of (A): the bare GCE (a) and the GNP modified GCE (b), (B): the GCE/Ru(bpy)$_3^{2+}$ modified electrode (a) and the GCE/Ru(bpy)$_3^{2+}$/GNP modified electrode (b) in 0.05 M H_2SO_4 solution at a scan rate of 100 mV s^{-1}.

Ru(bpy)$_3^{2+}$ modification effect. As shown in Fig. 2C, the size of the GNPs was uniform, and they were well distributed on the surface of GCE. After electrodeposition of the Ru(bpy)$_3^{2+}$ complex and GNPs on the surface of GCE, the SEM image (Fig. 2D) of the GCE/Ru(bpy)$_3^{2+}$/GNPs electrode showed that the Ru(bpy)$_3^{2+}$ complex and GNPs were steadily and uniformly immobilized on the surface of GCE.

3.2 Characterization of the biosensing electrode impedance

Electrochemical impedance spectroscopy (EIS) was adopted to monitor the fabrication processes of the biosensing electrode and characterize the impedance feature of nanopatterned GCE with Ru(bpy)$_3^{2+}$ complex molecules and GNPs. In the form of a Nyquist plot, Fig. 3 shows the impedance spectra obtained in the investigation. The bare GCE gave an almost linear arc plot with a micro radian in high frequency region and behaved as an ideal conductor (curve a), indicating a very fast electron transfer process of $[Fe(CN)_6]^{3-/4-}$. The immobilization of Ru(bpy)$_3^{2+}$/GNPs on the GCE affected the impedance feature of the electrode and showed a larger charge transfer resistance (R_{ct}) than the bare GCE (curve b). After the self-assembly of the thiolated-DNA strands, owing to the strong π–π interactions of ssDNA with Fc–GNs, Fc–GNs could be preferentially adsorbed on the ssDNA and highly enhance the electron transfer process of $[Fe(CN)_6]^{3-/4-}$. Therefore, a distinct decrease in electrochemical impedance can also be observed (curve c). The conformational transition of T-rich ssDNA induced by Hg^{2+} led to the desorption of Fc–GNs from double-stranded DNA (dsDNA) after the biosensing electrode is incubated in a certain concentration of Hg^{2+} for a period of time. It is obvious that the conformational transition could produce negative impedance performance and there is a slight increase in impedance (curve d).

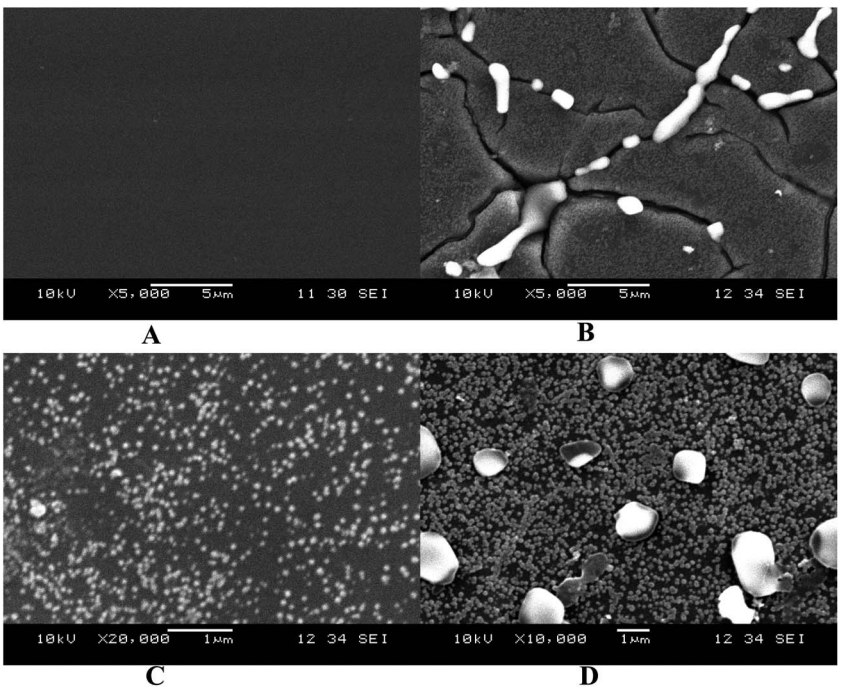

Fig. 2 SEM images of bare GC electrode surface (A), GCE/Ru(bpy)$_3^{2+}$ modified electrode (B), GNP modified GCE (C) and the GCE/Ru(bpy)$_3^{2+}$/GNP modified electrode (D).

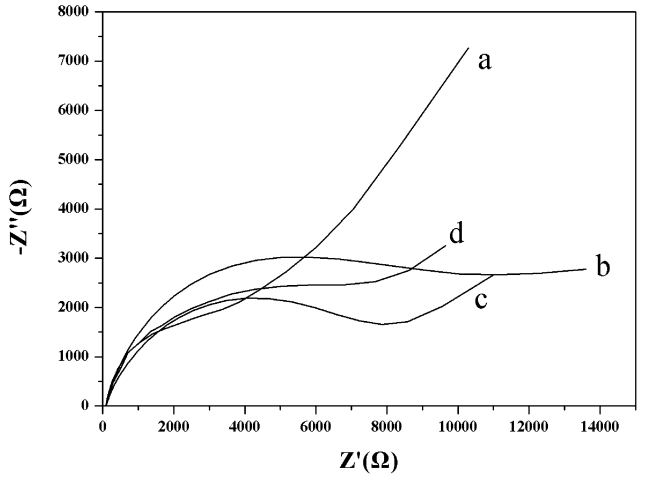

Fig. 3 Nyquist plot for electrochemical impedance measurements in 5.0 mM $[Fe(CN)_6]^{3-/4-}$ solution for the bare GCE (a), the GCE/$Ru(bpy)_3^{2+}$/GNP electrode (b), the Fc–GN modified GCE biosensor (c) and GCE biosensor after binding with Hg^{2+} (d).

3.3 Optimum conditions

In order to obtain the optimal conditions, several impact factors were optimized. We investigated the incubation time of the ECL biosensor electrode with Hg^{2+}, the pH of the test solution and the salt concentration of the PBS.

3.3.1 Incubation time. The effect of the incubation time on the performance of the biosensing electrode at Hg^{2+} concentrations of 0.05, 1 and 100 nM is shown in Fig. 4. As the incubation time increased, the ECL intensity change (ΔI_{ECL}) increased rapidly and reached a plateau after 30 min, suggesting that the T–Hg^{2+}–T stands was formed gradually and an almost complete binding reached. Therefore, 30 min was chosen for further experiments.

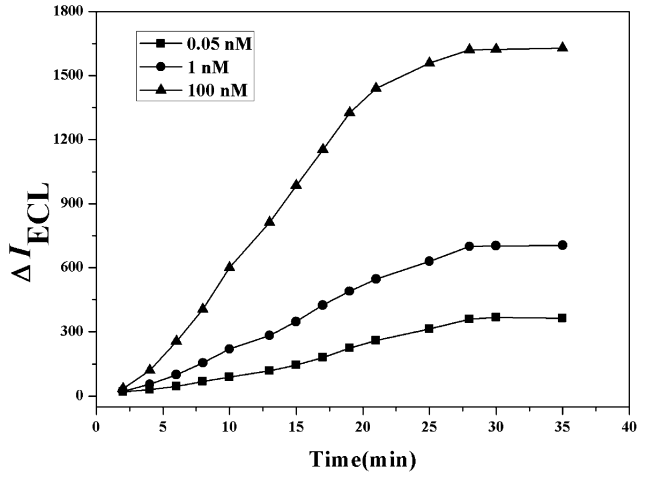

Fig. 4 Incubation time of ECL biosensing electrode with Hg^{2+} at concentrations of 0.05 nM, 1 nM and 100 nM. ECL intensity was measured in 0.1 M PBS (pH 7.50, 0.10 M NaCl + 0.10 M NaH_2PO_4/Na_2HPO_4) containing 0.1 M TPrA. Scan rate: 100 mV s^{-1}, scan range: 0.2–1.25 V.

3.3.2 pH and the concentration of NaCl. To investigate the effect of pH on the ECL intensity, the test solutions at diverse pH values (5.5 to 9.0 in intervals of 0.5, PBS: 0.10 M NaCl + NaH_2PO_4/Na_2HPO_4) were investigated. The ECL curves were measured in PBS containing 0.1 M TPrA after the Fc–GNs modified GCE biosensor was immersed in 100 nM Hg^{2+} solution. As shown in Fig. 5A, the best test solution was obtained at pH 7.50. This was probably due to the fact that the Hg^{2+} exhibits weak coordination with DNA thymine (T) bases in an acidic or alkalescent solution.

The concentration of NaCl in the PBS was very important to the activity of DNA, while the activity of DNA could affect the performance of the biosensing electrode. Therefore, the concentration of NaCl played a dominant role in the detection. The ECL determinations of the biosensing electrode were performed in PBS (pH 7.50, 0.10 M NaH_2PO_4/Na_2HPO_4 + NaCl) containing 0.1 M TPrA after the Fc–GN modified GCE biosensor was immersed in 100 nM Hg^{2+} solution. As shown in Fig. 5B, the ECL intensity was enhanced as a higher concentration of NaCl was added to the PBS and reached a peak at the concentration of 0.1 M. Thus, 0.1 M was selected as the optimal concentration of NaCl for further experiments.

3.4 Stability and reproducibility of the Hg^{2+} biosensor

The ECL method was used to prove that the monolayer of ssDNA probe was stably fabricated on the modified GCE in the 0.10 M PBS (pH 7.50, 0.10 M NaCl + 0.10 M NaH_2PO_4/Na_2HPO_4) containing 0.10 M TPrA using a linear potential scan technique. To test the quencher function of $Ru(bpy)_3^{2+}$ complex and Fc–GNs, a 28-*mer*-DNA, which is a T-rich fragment, was used to form a linear ssDNA and immobilized on the GNPs. Fc–GNs could be strongly adsorbed on the ssDNA due to strong π–π interactions, resulting in effective quenching of the ECL intensity of the $Ru(bpy)_3^{2+}$ complex. Fig. 6 shows that the $Ru(bpy)_3^{2+}$ complex electrodeposited on the GCE results in an obvious ECL signal response (curve b) in contrast with the bare GCE (curve a). After adsorbing the Fc–GNs, a striking decrease in ECL signal is found for the quenching effect of Fc to $Ru(bpy)_3^{2+}$ (curve c). The biosensor after incubation in a certain concentration of Hg^{2+} could give an obvious enhanced ECL signal response (curve d). The result can be explained as that the Hg^{2+} induced the conformational transition of T-rich ssDNA and then the quenching effect of Fc to $Ru(bpy)_3^{2+}$ became weaker because of desorption of Fc–GNs from dsDNA. Furthermore, as shown in the inset of Fig. 6, continuous CV scanning of the electrodes can give a balanced ECL intensity, indicating that the biosensor has acceptable reliability and stability, and the $Ru(bpy)_3^{2+}$ complex molecules were anchored on the GCE in the form of GCE/$Ru(bpy)_3^{2+}$ without $Ru(bpy)_3^{2+}$ complex molecules escaping from the glassy carbon surface of the GCE. The reproducibility of the biosensor was evaluated by analysis of the same concentration of Hg^{2+} (10 nM) using five biosensors under the same conditions. All biosensors exhibited close ECL responses, and a relative standard deviation (RSD) of 3.5% was obtained, which indicated that the reproducibility of the proposed biosensor was acceptable.

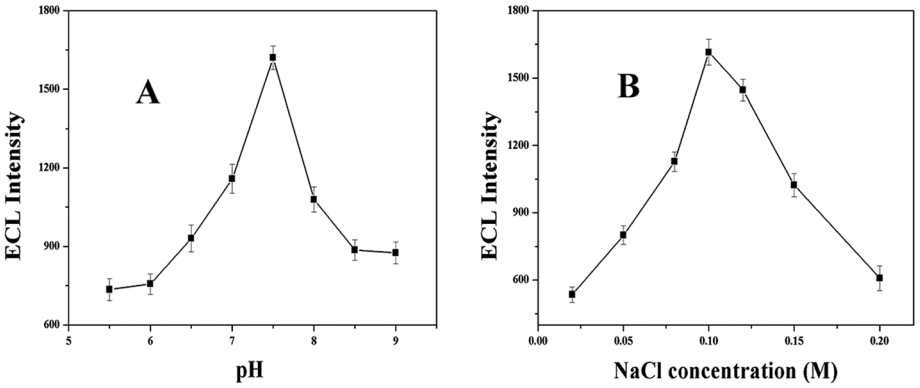

Fig. 5 The effect of pH (A) and NaCl concentration (B). (A): ECL intensity was measured in PBS (0.10 M NaCl + NaH_2PO_4/Na_2HPO_4) containing 0.1 M TPrA. Scan rate: 100 mV s^{-1}, scan range: 0.2–1.25 V. (B): ECL intensity was measured in PBS (NaCl + 0.10 M NaH_2PO_4/Na_2HPO_4) containing 0.1 M TPrA. Scan rate: 100 mV s^{-1}, scan range: 0.2–1.25 V.

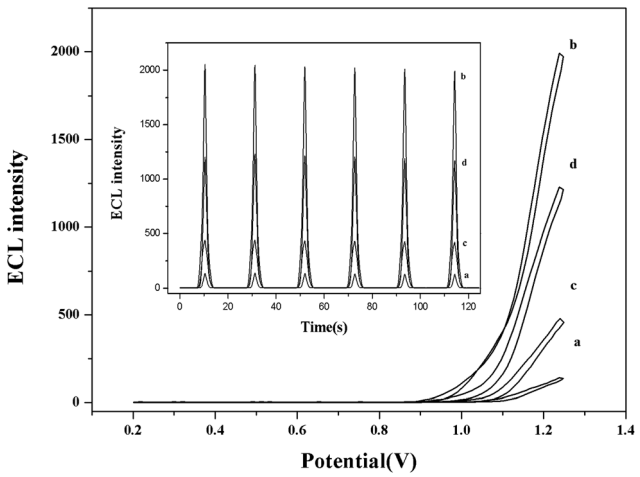

Fig. 6 ECL intensity *vs.* potential curves for the bare GCE (a), the GCE/$Ru(bpy)_3^{2+}$/GNP electrode (b), the Fc–GN modified GCE biosensor (c) and GCE biosensor after binding with Hg^{2+} (d). Inset: ECL intensity *vs.* time curves for the biosensor under continuous CV for six cycles. ECL curves were measured in 0.1 M PBS (pH 7.50, 0.10 M NaCl + 0.10 M NaH_2PO_4/Na_2HPO_4) containing 0.1 M TPrA. Scan rate: 100 mV s^{-1}, scan range: 0.2–1.25 V.

3.5 Sensitivity and selectivity of the Hg^{2+} biosensor

Under the optimized test conditions, the sensitivity of ECL biosensors was assessed by measuring the dependence of the increased ΔI_{ECL} upon the concentration of Hg^{2+}. As shown in Fig. 7, the ECL intensity was enhanced when a higher concentration of Hg^{2+} was used for binding the T-rich ssDNA, and the ΔI_{ECL} was found to be logarithmically related to the concentration of Hg^{2+} in a range from 0.05 nM to 100 nM (inset of Fig. 7). The regression equation was $\Delta I_{ECL} = 371 \lg C_{Hg^{2+}} + 4226.6$ with a regression coefficient of 0.9968 and detection limit of 18 pM, which is defined as the concentration corresponding to the mean blank value plus 3 standard deviations. This limit of detection (LOD) is 3 orders of magnitude lower than the Maximum Contaminant Level in drinking water set forth by the United States Environmental Protection Agency (USEPA) in the Clean Water Act of 2 ppb (10 nM). The performance of different Hg^{2+} sensors[31–35] is summarized in Table 1, which demonstrates that the detection limit of 18 pM in our work is highly sensitive.

The selectivity of the biosensor was examined by incubating the biosensor in the aqueous solutions containing Hg^{2+}, while the control experiments were performed using various metal ions like Cu^{2+}, Zn^{2+}, Ni^{2+}, Cd^{2+}, Mg^{2+}, Fe^{2+}, Ba^{2+}, Pb^{2+}, Cr^{3+}, Co^{2+}, Mn^{2+}, Fe^{3+}, Al^{3+} and Ca^{2+} at a concentration of 500 nM and Hg^{2+} at 10 nM. As shown in Fig. 8, the biosensor showed significant ECL intensity in response to Hg^{2+}, but hardly exhibited substantial responses to other metal ions, suggesting that the biosensor possessed an excellent selective response to Hg^{2+} against other environmentally relevant metal ions. Besides, we had performed an experiment with natural water samples, and the determination of Hg^{2+} concentration was performed by the standard addition method. As shown in Table S1,† we observed that the results obtained in natural water

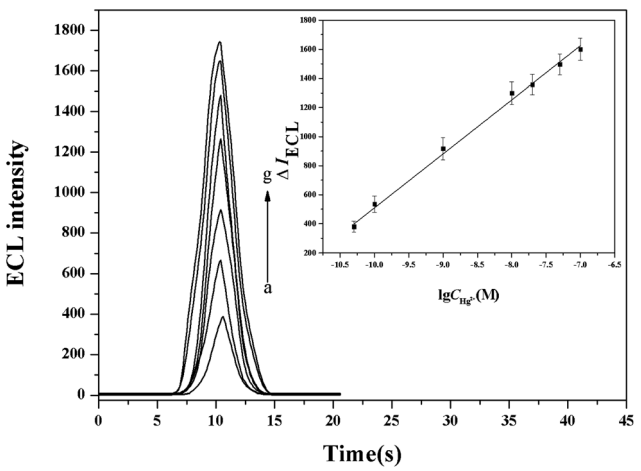

Fig. 7 ECL intensity–time curves for the biosensor binding with various concentration of Hg^{2+}. The concentrations of Hg^{2+} were 0.05 nM (a), 0.1 nM (b), 1 nM (c), 10 nM (d), 20 nM (e), 50 nM (f) and 100 nM (g). Inset: the calibration curve of the ECL response as a function of the concentration of Hg^{2+}. Error bars represent the standard deviation of five parallel experiments.

Table 1 Comparison of the sensitivity of different Hg^{2+} sensors

Detection method	Linear range	Limit of detection	Reference
Electrochemical method with Au nanoparticle-based signal amplification	1 nM–0.1 μM	0.5 nM	31
Electrochemical sensor based on ferrocene-labeled DNA	0.1–2 μM	0.1 μM	32
Electrochemical sensor based on the cooperation of proximate poly-T oligonucleotides	1 nM–2 μM	0.5 nM	33
Electrochemiluminescent biosensor using $Ru(bpy)_3^{2+}$-doped silica nanoparticles	5–500 nM	2.3 nM	34
Electrochemiluminescent method with $Ru(phen)_3^{2+}$ as the ECL probe	0.02–15 nM	20 pM	35
Electrochemiluminescent biosensor based on DNA-modified electrode and graphene *via* π–π interaction	0.05–100 nM	18 pM	This work

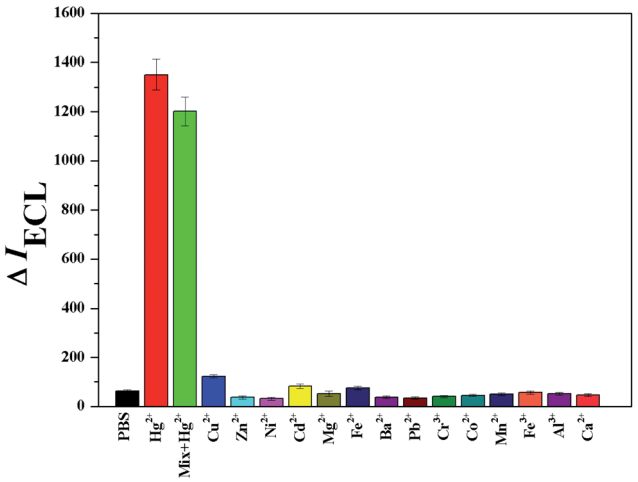

Fig. 8 Effects of various metal ions and a mixture of metal ions (500 nM each for Cu^{2+}, Zn^{2+}, Ni^{2+}, Cd^{2+}, Mg^{2+}, Fe^{2+}, Ba^{2+}, Pb^{2+}, Cr^{3+}, Co^{2+}, Mn^{2+}, Fe^{3+}, Al^{3+}, Ca^{2+} and 10 nM for Hg^{2+}) on the ECL signal response measured by the optimal ECL biosensor. Error bars represent the standard deviation of three repetitive experiments.

samples showed good recovery values (97.78–101.89%), which confirmed that the interferences in water samples could be neglected and the developed biosensor showed good selectivity for Hg^{2+}.

3.6 Direct detection of Hg^{2+} in water samples

The applications of the biosensor were evaluated for determination of Hg^{2+} in natural water. The concentration of Hg^{2+} was determined by the biosensing method as well as AFS method. The water samples were collected in the Xinhua River and Niutianyang Bay in Shantou, China. The samples collected were filtered through 0.2 μm membranes to remove impurities and diluted with an equal volume of PBS (pH 7.50, 0.10 M NaCl + 0.10 M NaH_2PO_4/Na_2HPO_4). The results are summarized in Table 2 and showed good agreement with those achieved by using the standard AFS method.

Table 2 Determination of the concentrations of Hg^{2+} in water samples using the proposed biosensing method and AFS[a] method

Water sample	Biosensing method (nM)	AFS method (nM)	Relative deviation (%)
Xinhua River 1	68.34 ± 4.05	69.26 ± 3.98	−1.36
Xinhua River 2	92.78 ± 8.53	90.84 ± 9.08	2.37
Niutianyang Bay 1	106.86 ± 7.89	110.12 ± 5.68	−3.84
Niutianyang Bay 2	143.67 ± 9.64	141.79 ± 7.31	2.03

[a] All values were obtained as average of three repetitive determinations plus standard deviation.

4. Conclusions

In conclusion, a solid-state ECL biosensor for the highly sensitive and selective detection of Hg^{2+} in aqueous solution has been developed. The $Ru(bpy)_3^{2+}$ complex was employed as an ECL label and strongly bonded on the surface of highly oxidized GC electrodes by a brief potentiostatic approach, and the biosensor showed excellent and stable ECL intensity. The quenching pattern of Fc–GNs to $Ru(bpy)_3^{2+}$ *via* π–π interaction between nucleotides and Fc–GNs simplifies the experimental design and exerts a stable quenching effect on $Ru(bpy)_3^{2+}$. Moreover, the optimized distribution and orientation of ssDNA, which was well controlled by the GNPs, played a very important role in the sensitivity of the biosensor to Hg^{2+}. In our present work, the presented biosensor has a detection limit of 18 pM, which is much lower than the USEPA limit of Hg^{2+} in drinkable water (<10 nM). In addition, this design of the biosensor does not require costly equipment and sophisticated sample pretreatment. In summary, a cost-effective and rapid method presented in our study makes it possible for on-site detection of Hg^{2+} in actual environmental water samples.

Acknowledgements

We acknowledge financial support for this work from Research Start-up Funding of Shantou University (no. NTF10002), the Natural Science Foundation of Guangdong Province (no. S2011010005208), the National Natural Science Foundation of China (no. 51272152/E0208) and the Guangdong High Education Fund of Science and Technology Innovation (no. 2013KJCX0078).

References

1 Q. R. Wang, D. Kim, D. D. Dionysiou, G. A. Sorial and D. Timberlake, *Environ. Pollut.*, 2004, **131**, 323–336.
2 P. W. Davidson, G. J. Myers and B. Weiss, *Pediatrics*, 2004, **113**, 1023–1029.
3 Y. Q. Lai, Y. Y. Ma, L. P. Sun, J. Jia, J. Weng, N. Hu, W. Yang and Q. Q. Zhang, *Electrochim. Acta*, 2011, **56**, 3153–3158.
4 V. L. Dressler, F. G. Antes, C. M. Moreira, D. Pozebon and F. A. Duarte, *Int. J. Mass Spectrom.*, 2011, **307**, 149–162.
5 Y. Miyake, H. Togashi, M. Tashiro, H. Yamaguchi, S. Oda, M. Kudo, Y. Tanaka, Y. Kondo, R. Sawa, T. Fujimoto, T. Machinami and A. Ono, *J. Am. Chem. Soc.*, 2006, **128**, 2172–2173.
6 Y. Tanaka, S. Oda, H. Yamaguchi, Y. Kondo, C. Kojima and A. Ono, *J. Am. Chem. Soc.*, 2007, **129**, 244–245.
7 X. Y. Wang, W. Yun, P. Dong, J. M. Zhou, P. G. He and Y. Z. Fang, *Langmuir*, 2008, **24**, 2200–2205.
8 M. M. Richter, *Chem. Rev.*, 2004, **104**, 3003–3036.
9 W. Miao, *Chem. Rev.*, 2008, **108**, 2506–2553.
10 H. Dai, Y. M. Wang, X. P. Wu, L. Zhang and G. N. Chen, *Biosens. Bioelectron.*, 2009, **24**, 1230–1234.
11 Z. H. Guo, Y. Shen, M. K. Wang, F. Zhao and S. J. Dong, *Anal. Chem.*, 2004, **76**, 184–191.
12 X. P. Sun, Y. Du, L. X. Zhang, S. J. Dong and E. K. Wang, *Anal. Chem.*, 2007, **79**, 2588–2592.
13 X. Zhang and A. J. Bard, *J. Phys. Chem.*, 1988, **92**, 5566–5569.
14 I. Rubinstein and A. J. Bard, *J. Am. Chem. Soc.*, 1981, **103**, 5007–5013.
15 M. M. Collinson, B. Novak, S. A. Martin and J. S. Taussig, *Anal. Chem.*, 2000, **72**, 2914–2918.
16 W. H. Gao, Y. S. Chen, J. Xi, A. Zhang, Y. W. Chen, F. S. Lu and Z. G. Chen, *Sens. Actuators, B*, 2012, **171–172**, 1159–1165.
17 J. Premkumar and S. B. Khoo, *Electrochem. Commun.*, 2004, **6**, 984–989.
18 D. Li, M. B. Muller, S. Gilje, R. B. Kaner and G. G. Wallace, *Nat. Nanotechnol.*, 2008, **3**, 101–105.
19 Y. Y. Shao, J. Wang, H. Wu, J. Liu, I. A. Aksay and Y. H. Lin, *Electroanalysis*, 2010, **22**, 1027–1036.
20 H. Y. Mao, S. Laurent, W. Chen, O. Akhavan, M. Imani, A. A. Ashkaran and M. Mahmoudi, *Chem. Rev.*, 2013, **113**, 3407–3424.
21 K. Wang, Q. Liu, Q. M. Guan, J. Wu, H. N. Li and J. J. Yan, *Biosens. Bioelectron.*, 2011, **26**, 2252–2257.
22 D. B. Zhu, J. F. Liu, Y. B. Tang and D. Xing, *Sens. Actuators, B*, 2010, **149**, 221–225.
23 C. L. Sun, H. H. Lee, J. M. Yang and C. C. Wu, *Biosens. Bioelectron.*, 2011, **26**, 3450–3455.
24 Y. J. Li, W. Gao, L. J. Ci, C. M. Wang and P. M. Ajayan, *Carbon*, 2010, **48**, 1124–1130.
25 T. Kuila, S. Bose, P. Khanra, A. K. Mishra, N. H. Kim and J. H. Lee, *Biosens. Bioelectron.*, 2011, **26**, 4637–4648.
26 L. Wang, M. Xu, L. Han, M. Zhou, C. Z. Zhu and S. J. Dong, *Anal. Chem.*, 2012, **84**, 7301–7307.
27 W. H. Gao, A. Zhang, Y. S. Chen, Z. X. Chen, Y. W. Chen, F. S. Lu and Z. G. Chen, *Biosens. Bioelectron.*, 2013, **49**, 139–145.
28 W. S. Hummers and R. E. Offeman, *J. Am. Chem. Soc.*, 1958, **80**, 1339.
29 L. S. Fan, Q. X. Zhang, K. K. Wang, F. H. Li and L. Niu, *J. Mater. Chem.*, 2012, **22**, 6165–6170.
30 S. J. Wang, M. T. Neshkova and W. J. Miao, *Electrochim. Acta*, 2008, **53**, 7661–7667.
31 R. M. Kong, X. B. Zhang, L. L. Zhang, X. Y. Jin, S. Y. Huan, G. L. Shen and R. Q. Yu, *Chem. Commun.*, 2009, **37**, 5633–5635.
32 D. Han, Y. Kim, J. Oh, T. H. Kim, R. K. Mahajan, J. S. Kim and H. Kim, *Analyst*, 2009, **134**, 1857–1862.
33 S. J. Liu, H. G. Nie, J. H. Jiang, G. L. Shen and R. Q. Yu, *Anal. Chem.*, 2009, **81**, 5724–5730.
34 X. Zhu, L. F. Chen, Z. Y. Lin, B. Qiu and G. N. Chen, *Chem. Commun.*, 2010, **46**, 3149–3151.
35 C. X. Tang, Y. Zhao, X. W. He and X. B. Yin, *Chem. Commun.*, 2010, **46**, 9022–9024.

